The deposition ice nucleation and immersion freezing potential of amorphous secondary organic aerosol: Pathways for ice and mixed-phase cloud formation

Authors: B. Wang, A.T. Lambe, P. Massoli, T.B. Onasch, Paul Davidovits, D.R. Worsnop, D.A. Knopf

The deposition ice nucleation and immersion freezing potential of amorphous secondary organic aerosol: Pathways for ice and mixed-phase cloud formation

Bingbing Wang,[1,2] Andrew T. Lambe,[3,4] Paola Massoli,[4] Timothy B. Onasch,[3,4] Paul Davidovits,[3] Douglas R. Worsnop,[4] and Daniel A. Knopf[l]

[1]   Secondary organic aerosol (SOA) generated from the oxidation of organic gases are ubiquitous in the atmosphere, but their interaction with water vapor and their ice cloud formation potential at low temperatures remains highly uncertain. We report on onset conditions of water uptake and ice nucleation by amorphous SOA particles generated from the oxidation of naphthalene with OH radicals. Water uptake above 230 K was governed by the oxidation level of the SOA particles expressed as oxygen-to-carbon (O/C) ratio, followed by moisture-induced phase transitions and immersion freezing. For temperatures from 200 to 230 K, SOA particles nucleated ice via deposition mode from supersaturated water vapor independent of O/C ratio at relative humidity with respect to ice (RH_{ice}) ~10–15% below homogeneous ice nucleation limits. The glass transition temperature (T_g) for the amorphous SOA particles was derived as a function of two parameters: (1) relative humidity (RH) with respect to water and (2) oxidation level of the SOA. The data show that particle phase and viscosity govern the particles' response to temperature and RH and provide a straightforward interpretation for the observed different heterogeneous ice nucleation pathways and water uptake by the laboratory-generated SOA and field-collected particles. Since SOA particles undergo glass transitions, these observations suggest that atmospheric SOA are potentially important for ice cloud formation and climate.

Citation: Wang, B., A. T. Lambe, P. Massoli, T. B. Onasch, P. Davidovits, D. R. Worsnop, and D. A. Knopf (2012), The deposition ice nucleation and immersion freezing potential of amorphous secondary organic aerosol: Pathways for ice and mixed-phase cloud formation, *J. Geophys. Res.*, *117*, D16209, doi:10.1029/2012JD018063.

1.   Introduction

[2]   Prediction of atmospheric ice formation remains one of the largest uncertainties in climate models. This may be due to the different scales involved in microphysics and climate models and the various ice formation pathways [*Baker and Peter*, 2008]. Ice nucleation can occur through homogenous freezing of aqueous droplets below ~238 K and heterogeneously on the surface of airborne particles acting as ice nuclei (IN) at higher temperatures and lower supersaturation with respect to ice [*Pruppacher and Klett*, 1997]. Hence, IN have a higher propensity to initiate ice crystal formation and to impact cirrus (containing ice crystals) and mixed-phase (containing ice crystals and aqueous droplets) cloud formation. Cirrus clouds cover approximately 20% of the Earth's surface and can have a net positive radiative forcing [*Chen et al.*, 2000]. Mixed-phase clouds can also alter radiative forcing due to sedimentation and water vapor scavenging by ice crystals, thereby impacting cloud lifetime, albedo, and precipitation, which in turn affects the hydrological cycle [*Storelvmo et al.*, 2011]. Mixed-phase clouds have been observed for temperatures as low as about −40° [e.g., *Shupe et al.*, 2006; *de Boer et al.*, 2011].

[3]   Aerosol particles may adopt different physical states including crystalline, liquid, and amorphous semi-solid and solid (i.e. glassy) states [*Martin*, 2000; *Mikhailov et al.*, 2009; *Koop et al.*, 2011]. An amorphous glass exhibits similar mechanical properties as a solid, but lacks the long-range molecular order which is typical of the crystalline state [*Debenedetti and Stillinger*, 2001]. Ice nucleation is a very selective process and one of the main requirements for a particle acting as IN is to provide a solid surface as the center

[1]Institute for Terrestrial and Planetary Atmospheres, School of Marine and Atmospheric Sciences, State University of New York at Stony Brook, Stony Brook, New York, USA.
[2]Now at William R. Wiley Environmental Molecular Sciences Laboratory, Pacific Northwest National Laboratory, Richland, Washington, USA.
[3]Chemistry Department, Boston College, Chestnut Hill, Massachusetts, USA.
[4]Aerodyne Research Inc., Billerica, Massachusetts, USA.

Corresponding author: D. A. Knopf, Institute for Terrestrial and Planetary Atmospheres, School of Marine and Atmospheric Sciences, State University of New York at Stony Brook, Stony Brook, NY 11794, USA. (daniel.knopf@stonybrook.edu)

of ice nucleation [*Pruppacher and Klett*, 1997]. Thus the ice nucleation pathway and efficiency of particles acting as IN can be governed by particle phase state which in turn also depend on particle composition, mixing state, and the surrounding conditions [*Martin*, 2000; *Marcolli et al.*, 2004; *Abbatt et al.*, 2006; *Zobrist et al.*, 2006; *Murray*, 2008; *Zobrist et al.*, 2008; *Mikhailov et al.*, 2009; *Murray et al.*, 2010; *Koop et al.*, 2011; *Baustian et al.*, 2012; B. Wang et al., Heterogeneous ice nucleation and water uptake by field-collected atmospheric particles below 273 K, submitted to *Journal of Geophysical Research*, 2012].

[4] It is commonly assumed that inorganic particles such as mineral dust and solid ammonium sulfate, both ubiquitous in the atmosphere, represent important IN [e.g., *DeMott et al.*, 2003; *Abbatt et al.*, 2006; *Eastwood et al.*, 2008; *Wise et al.*, 2010]. However, the ubiquitous organic aerosols including SOA formed from the oxidation of gas-phase precursors [*Kanakidou et al.*, 2005; *Hallquist et al.*, 2009] may also play an important role in ice formation for the following reasons. First, the ability of SOA to form cloud condensation nuclei (CCN) above the melting point of ice is well documented, suggesting that SOA might also act as IN after initial water uptake for temperatures below the melting point of ice. Second, and more importantly, recent studies have shown that SOA generated from several biogenic and anthropogenic gas-phase precursors are characterized by an amorphous solid or semi-solid phase [*Virtanen et al.*, 2010; *Koop et al.*, 2011; *Virtanen et al.*, 2011; *Saukko et al.*, 2012a, 2012b]. Finally, potential SOA surrogate materials in a solid state have been shown to induce heterogeneous ice nucleation [*Murray et al.*, 2010; *Wagner et al.*, 2012; *Wilson et al.*, 2012]. The amorphous solid state of SOA particles may facilitate heterogeneous ice nucleation via the immersion or deposition mode by acting as IN. In immersion freezing, ice forms on IN in a supercooled aqueous droplet, whereas for deposition ice nucleation, ice forms on IN from supersaturated water vapor [*Pruppacher and Klett*, 1997].

[5] Fundamental properties of organic particles, including SOA, that influence IN efficiency are the glass transition temperature (T_g) and the bulk water diffusion coefficient (D_{H_2O}) in the organic matrix, which determine their water content and phase states, i.e. liquid, amorphous semi-solid, and solid. T_g is the temperature at which a transition between liquid/semi-solid and solid states occurs [*Debenedetti and Stillinger*, 2001; *Zobrist et al.*, 2008; *Koop et al.*, 2011; *Zobrist et al.*, 2011]. Thus, T_g can be used as a representative temperature below which an amorphous organic particle exhibits solid properties and above which the organic particle is likely to be in a semi-solid or liquid state. Various factors may affect or control T_g of organic particles including the molar mass, oxidation level (O/C ratio), mixing state, and ambient relative humidity (*RH*) [*Koop et al.*, 2011]. *Koop et al.* [2011] suggested that, *RH*, which equals water activity at equilibrium and thus defines the water content of organic particle, is also very important to characterize the particle state. Water, which exhibits a T_g of 136 K, can serve as a plasticizer in organic particles and thus it reduces the T_g of the pure dry organic component, $T_g(RH = 0\%)$ [*Koop et al.*, 2011]. Organic particles with higher water content will exhibit lower T_g.

[6] Previous cirrus and mixed-phase cloud studies have shown that ice crystal residues can contain organic materials [*Chen et al.*, 1998; *DeMott et al.*, 2003; *Cziczo et al.*, 2009; *Froyd et al.*, 2009; *Prenni et al.*, 2009a; *Froyd et al.*, 2010], but the exact effects of organics on ice nucleation are not clear. So far only a few studies have investigated the ice nucleation efficiency of SOA particles and for a limited temperature range [*Wagner et al.*, 2007; *Prenni et al.*, 2009b; *Möhler et al.*, 2008]. *Möhler et al.* [2008] showed that at 205 K the coating of SOA stemming from the reaction of α-pinene with O_3 suppressed ice nucleation of mineral dust and that pure SOA particles are not efficient IN [*Wagner et al.*, 2007; *Möhler et al.*, 2008]. *Prenni et al.* [2009b] investigated the ice nucleation of SOA particles generated by the ozonolysis of volatile organic mixtures and did not observe ice nucleation in detectable quantities at 243 K. Several studies have investigated the ice nucleation ability of organic particle surrogates which have potential to exist in an amorphous solid state [*Murray et al.*, 2010; *Wagner et al.*, 2012; *Wilson et al.*, 2012]. *Murray et al.* [2010] have shown that pure citric acid particles nucleated ice heterogeneously below 212 K when the particle adopted a solid state and homogeneously above 212 K when it existed in an aqueous state. Most recently, *Wilson et al.* [2012] and *Wagner et al.* [2012] investigated the ice nucleation ability of pure organic compounds including raffinose, 4-hydroxy-3-methoxy-DL-mandelic acid (HMMA), and levoglucosan and a mixture of raffinose with five dicarboxylic acids and ammonium sulfate (Raffinose/M5AS). They showed that these four particle types nucleated ice heterogeneously below the respective T_g [*Zobrist et al.*, 2008].

[7] In this study, the onset conditions of water uptake and heterogenous ice nucleation by laboratory-generated amorphous SOA with different O/C ratios were investigated as a function of temperature as low as 200 K and RH_{ice} up to water saturation. Complementary analytical techniques were used to characterize the SOA particles including the particle phase, particle density, and hygroscopicity. The T_g for the investigated SOA particles was estimated as a function of *RH*. These T_g values were used to interpret the water uptake and heterogenous ice nucleation of the SOA and field-collected organic-dominated particles.

2. Experimental Setup

2.1. Generation and Collection of SOA Particles

[8] SOA particles were generated via gas-phase oxidation of naphthalene with OH radicals followed by homogeneous nucleation of gas phase products in a Potential Aerosol Mass (PAM) flow reactor [*Kang et al.*, 2007; *Lambe et al.*, 2011a]. Figure 1 shows a schematic of the laboratory setup used for SOA particle generation and collection. Input gas lines 1 and 2 provided carrier gases (N_2 and O_2) and OH radical precursors (O_3 and H_2O) with a total flow rate of 9.0 liter per minute (lpm). Line 3 provided the SOA precursor, in this case naphthalene, which was introduced into the PAM flow reactor in the gas phase by passing N_2 (0.015 lpm) over solid naphthalene enclosed in a Teflon tube. OH radicals were produced via the reaction $O_3 + h\nu \rightarrow O_2 + O(^1D)$ followed by the reaction $O(^1D) + H_2O \rightarrow 2OH$. O_3 was generated by irradiating O_2 with a mercury lamp ($\lambda = 185$ nm) outside the PAM reactor. The $O(^1D)$ atoms were produced by UV photolysis of O_3 inside the PAM reactor using four mercury lamps (BHK Inc.) with peak emission intensity at $\lambda = 254$ nm. These lamps
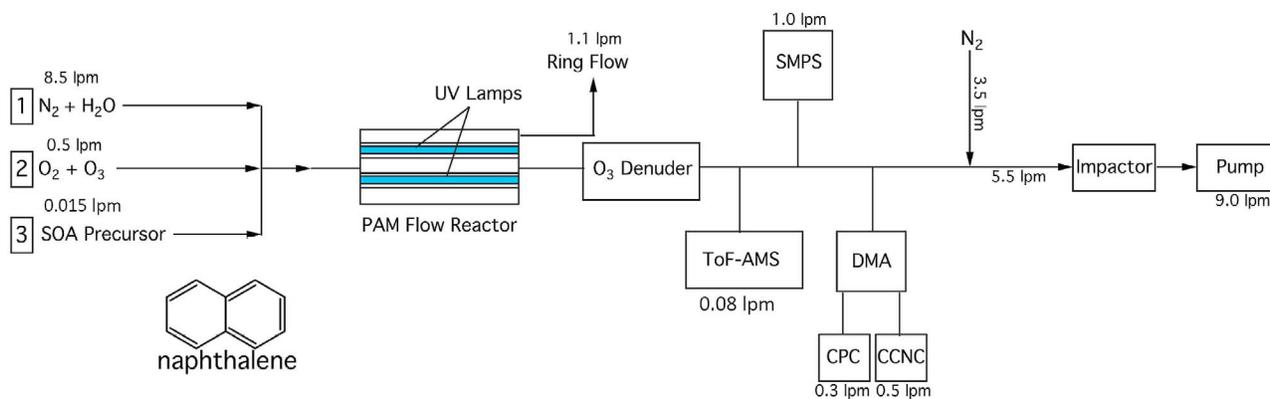
Figure 1. A schematic of the experimental setup for SOA sample generation and collection adapted from *Lambe et al.* [2011a]. As indicated, input lines 1 and 2 provided carrier gases (N_2 and O_2) and OH radical precursors (O_3 and H_2O). Line 3 provided naphthalene precursor to generate SOA. (lpm represents liter per minute).

were mounted in Teflon-coated quartz cylindrical sleeves and were continually purged with O_2. Water vapor was introduced using a heated Nafion membrane humidifier (Perma Pure LLC). The average gas-phase species residence time in the PAM reactor was approximately 100 s. The OH exposure, which is the product of the OH concentration and the average residence time in the PAM reactor, was obtained indirectly by measuring the decay of SO_2 due to reaction with OH. The OH concentration was varied by changing the UV light intensity through stepping the lamp voltages between 0 and 110 V. SO_2 calibration measurements were conducted as a function of UV lamp intensity and O_3 concentration [*Lambe et al.*, 2011b].

[9] SOA generation experiments were conducted at *RH* of ~35 ± 5% and at OH exposures (i.e. present OH concentration times exposure time) of ~2.8 × 10^{11}, 1.0 × 10^{12}, and 2.2 × 10^{12} molec cm^{-3} s corresponding to oxidation times of ~2, 8, and 17 days assuming 24-hour average ambient OH concentration of 1.5 × 10^6 molec cm^{-3} [*Mao et al.*, 2009]. While OH concentrations in these experiments (approximately 2.8 × 10^9 to 2.2 × 10^{10} molec cm^{-3}) are higher than ambient OH concentrations, the integrated OH exposures are similar. Previous work suggests that, to first order, extrapolation of flow tube reactor conditions (high [OH], short exposure times) to atmospheric conditions (low [OH], long exposure times) is reasonable [*Renbaum and Smith*, 2011]. For the water uptake and ice nucleation experiments, SOA particles were collected on hydrophobically coated glass plates using a four-stage Sioutas cascade impactor (SKC Inc.) as shown in Figure 1. The particles were collected on the fourth stage with 50% cut-off size of 0.25 μm at a total flow rate of 9.0 lpm.

2.2. Water Uptake and Ice Nucleation Experiments

[10] Onset conditions (temperature and RH_{ice}) of ice nucleation and water uptake by aerosol particles were determined using a controlled vapor cooling-stage microscope system consisting of an optical microscope (OM) and a custom-built ice nucleation cell (INC) described in detail elsewhere [*Knopf et al.*, 2010, 2011; *Wang and Knopf*, 2011]. The onset conditions for water uptake and the first ice nucleation event initiated by the deposited particles were

determined according to the changes in particle size and phase for temperatures as low as 200 K and RH_{ice} up to water saturation. SOA particles on a hydrophobically coated glass slide were exposed to a humidified flow of N_2 at constant dew point temperature. Water uptake and ice nucleation experiments were started at particle temperatures below expected particle glass transition temperature (see below) and at ice subsaturated conditions. Typical experimental trajectories are shown in Figures 2 and 3 in section 3. For these reasons the amorphous SOA particles were in a solid state at the beginning of the experiments. The particles were then cooled at a rate of 0.1 K min^{-1}, corresponding to an increase in RH_{ice} of ~2.3% to 1.5% per minute (corresponding to atmospherically relevant updraft velocities [*Kärcher and Ström*, 2003; *Kärcher and Lohmann*, 2003; *Kärcher et al.*, 2006]) for temperatures from 260 to 200 K, and exposed to ice supersaturation until ice formation or water uptake was observed. At the given temperature uncertainties of $\Delta T_d <$ ±0.15 K and $\Delta T_p <$ ±0.3 K, conservative (i.e. the maximum difference between T_d and T_p) RH_{ice} uncertainty is less than ±10% at 203 K and ±3% at 260 K. The entire experiment including ice formation, water uptake, and particle and dew point temperatures was recorded digitally for post analysis. Auxiliary material Figure S1 gives exemplary optical images showing water uptake, immersion freezing, and deposition ice nucleation.[1] Corresponding *RH* and RH_{ice} above the particles were derived from water partial pressure determined by dew point temperature and saturation vapor pressure at particle temperature [*Murphy and Koop*, 2005; *Wang and Knopf*, 2011]. Analysis of the digital images yields water uptake and ice nucleation onsets. The onset conditions for heterogeneous ice nucleation and water uptake by amorphous SOA particles were determined using two independent samples for each O/C ratio. At each temperature, the water uptake and ice nucleation experiments were repeated at least three times for each particle sample.

[11] The mean particle diameter (*D*), particle number density on substrate, and total particulate surface area of SOA samples available for the water uptake and ice

---

[1]Auxiliary materials are available in the HTML. doi:10.1029/2012JD018063.

Table 1. Particle Samples, Oxidation Level Expressed as O/C Ratio, Effective Particle Density (ρ), Mean Particle Hygroscopicity (κ), Upper Limit of the Glass Transition Temperature at Dry ($RH = 0\%$) Conditions, and Mean Values of Particle Diameter, Particle Number Density on Substrate (Num. Dens.), and Total Particulate Surface Area (Surf. Area) for Ice Nucleation Experiments

Sample	O/C Ratio[a]	ρ^b (g cm^{-3})	κ	$T_g (RH = 0\%)^c$ (K)	D^d (μm)	Num. Dens.[e] ($\times 10^4$ mm^{-2})	Surf. Area[f] ($\times 10^{-2}$ mm^2)
High O/C	1.0 ± 0.3	1.3 ± 0.3	0.22 ± 0.04	320 ± 10	0.7 ± 0.7	1.2 ± 0.3	1.1 ± 0.3
Medium O/C	0.54 ± 0.16	1.3 ± 0.3	0.24 ± 0.05	322 ± 11	1.1 ± 1.0	3.0 ± 0.2	5.4 ± 1.4
Low O/C	0.27 ± 0.08	1.3 ± 0.3	0.14 ± 0.03	312 ± 7	0.7 ± 0.8	3.9 ± 0.4	3.0 ± 0.8
CalNex	0.41 ± 0.12^g				0.3 ± 0.1	230	26 ± 4
SRFA[h]	0.57	1.47 ± 0.02	0.025–0.077	309	$(2.0$–$2.4) \pm 1.0$		1.4–3.8

[a]For SOA particles, uncertainty in O/C ratio was estimated to be ∼30% (upper limit) [*Massoli et al.*, 2010].

[b]For SOA particles, uncertainties in ρ [*DeCarlo et al.*, 2004] and κ [*Massoli et al.*, 2010] were estimated to be ∼20%.

[c]Conservative uncertainties were estimated with considerations of the uncertainties of ρ, κ, and RH ($\pm 5\%$ at generation conditions).

[d]Uncertainty represents one standard derivation (1σ).

[e]Particles smaller than ∼0.4 μm and ∼0.05 μm can't be detected or were considered using optical microscope (for SOA samples) and scanning electron microscopy (SEM, for CalNex sample), respectively. The presented particle number density should be considered as a lower limit. For SOA samples, the uncertainty represents the range in applied samples.

[f]Uncertainty represents the range of the applied SOA samples or uncertainty due to the resolution of optical microscope (∼0.2 μm at the magnification of 1130), whichever is larger. Uncertainty was estimated with consideration of ∼0.02 μm resolution of SEM for CalNex sample.

[g]P. L. Hayes et al. (Aerosol composition in Los Angeles During the 2010 CalNex Campaign Studied by High Resolution Aerosol Mass Spectrometry, submitted to *Journal of Geophysical Research*, 2012).

[h]Values were obtained from previous studies. See the text for more details.

nucleation experiments (Table 1) were determined using optical microscopy [*Wang and Knopf*, 2011]. The deposited particles were treated as hemispheres and the diameters were determined from the 2-dimension particle projected area (A), $D = 2(A/\pi)^{1/2}$. The total particle surface area (SA) available for the water uptake and ice nucleation experiments was derived from D, particle number density, and sample area exposed to the water vapor in the INC during the ice nucleation experiment (A_{ice}), $SA = 1/2\pi D^2 N A_{ice}$. Assumption of hemispheric particles results in a maximum particle surface area while the minimum value would be the 2-dimension projected area (i.e., $SA_{min} = 1/4\pi D^2 N A_{ice}$). The presented D values (Table 1) are higher than the mean volume-weighted mobility diameters determined from SMPS measurements (79–128 nm) most likely due to particle coagulation on the substrates before size investigation by optical microscope. Corresponding parameters determined by computer controlled scanning electron microscopy for organic-dominated ambient particles collected during the CalNex (California Research at the Nexus of Air Quality and Climate Change) campaign in 2010 are also listed in Table 1 [*Knopf et al.*, 2010; Wang et al., submitted manuscript, 2012]. The presented ice nucleation onsets were obtained for given total particle numbers and total particulate surface areas available in the ice nucleation experiments. According to classical nucleation theory and previous findings, it can be expected that the ice nucleation onsets change when sampling different total particle numbers and total particulate surface areas [*Pruppacher and Klett*, 1997; *Kanji et al.*, 2008; *Kanji and Abbatt*, 2010].

2.3. Characterization of SOA Particle Phase and Composition

[12] The phase of naphthalene SOA particles produced in the PAM reactor used in this work was measured using a novel low pressure impactor (LPI) technique to derive particle bounced fraction in a separate study [*Saukko et al.*, 2012b]. As described by *Saukko et al.* [2012a, 2012b], the core LPI components included a Nafion humidifier, a low pressure impactor with a polished steel substrate, and a CPC. The number concentration of size-selected SOA particles

was measured upstream and downstream of the impactor stage. The "bounced fraction" is defined as the ratio of concentrations after and before the impactor, divided by the same ratio with a baseline sample without the impaction substrate. Particles with higher bounced fraction possess higher viscosities than those with lower bounced fraction. The bounced fraction of crystallized (solid) and deliquesced (liquid) ammonium sulfate particles was about 0.8 and 0, respectively. The measured bounced fraction of naphthalene SOA particles was about 0.6 ± 0.2 below 50% RH, suggesting that the naphthalene SOA particles were characterized by an amorphous semi-solid phase [*Saukko et al.*, 2012a, 2012b].

[13] An Aerodyne compact time-of-flight aerosol mass spectrometer (c-ToF-AMS) [*Drewnick et al.*, 2005] was used to obtain aerosol mass spectra of SOA particles for the determination of particle oxidation level expressed as oxygen-to-carbon (O/C) ratio. In addition, Scanning Mobility Particle Sizer (SMPS) was used to measure the size distribution of generated SOA particles prior to collection. The CCN activation of size-selected SOA particles was measured with a Continuous Flow CCN Counter (CCNC, Droplet Measurement Technologies) [*Roberts and Nenes*, 2005; *Lance et al.*, 2006] to derive the particle hygroscopicity parameter.

[14] CCN number concentrations were measured with the CCNC and total particle number concentrations were measured with a condensation particle counter (CPC, TSI 3022A). CCN activation curves were generated by systematically varying the CCNC column temperature gradient to obtain controlled water vapor supersaturation between 0.1–1.5% or until 100% activation was reached, whichever occurred first. The water vapor supersaturation was calibrated using size-selected ammonium sulfate particles. The CCN hygroscopicity parameter of the SOA particles [*Petters and Kreidenweis*, 2007], κ, was calculated using the following equations:

$$\kappa = \frac{4A^3}{27D_d^3 ln^2 S_c}, \tag{1}$$

$$A = \frac{4\sigma_w M_w}{RT\rho_w}, \tag{2}$$
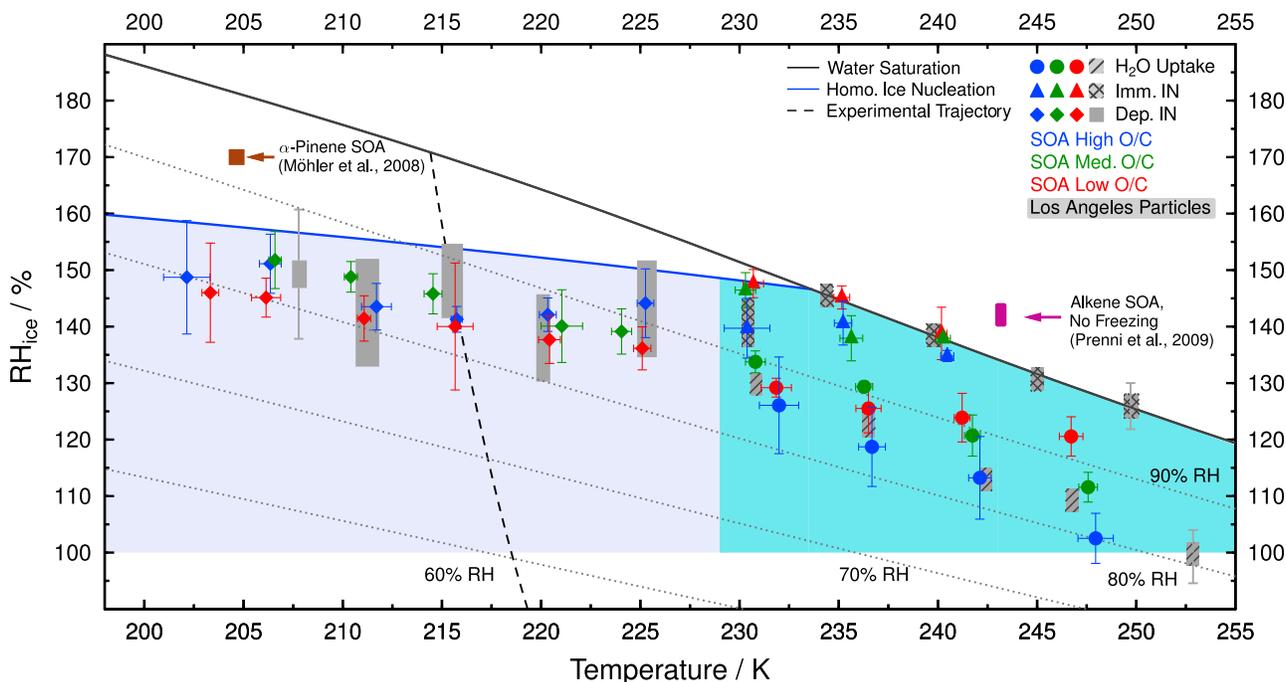
Figure 2. Experimentally determined mean onset conditions ($\pm 1\sigma$) of water uptake (circles), immersion freezing (triangles), deposition ice nucleation (diamonds) by laboratory-generated amorphous secondary organic aerosol (SOA) particles with high (1.0), medium (0.54), and low (0.27) O/C ratios are shown in blue, green, and red, respectively. The ranges of onset conditions for water uptake, immersion freezing, and deposition ice nucleation by ambient particles collected in Los Angeles during the CalNex field study are shown as shaded, hatched, and solid grey bars, respectively. Representative uncertainties are given on selected data points. The brown square indicates the onset of ice nucleation by SOA produced from ozonolysis of α-pinene [*Möhler et al.*, 2008] and the purple arrow indicates that no ice nucleation was observed for SOA produced from ozonolysis of a suite of alkene precursors [*Prenni et al.*, 2009b]. The bluish and grayish background indicate the temperature regime in which water uptake and immersion freezing and deposition ice nucleation are observed, respectively. The solid black line indicates water saturation (100% RH) and dotted lines indicate 90, 80, 70, and 60% RH. The dashed line indicates a typical experimental trajectory. The blue line indicates the homogeneous ice nucleation limit [*Koop et al.*, 2000].

where D_d is the dry diameter of the size-selected particles, S_c is critical saturation ratio, R is the universal gas constant, T is the sample temperature, and M_w, ρ_w, and σ_w are the molecular weight, density, and surface tension of water ($\sigma_w = 0.072$ J m^{-2}). The measured κ values were used to calculate the glass transition temperature of SOA, as discussed below.

3. Results and Discussion

3.1. Particle Characterization

[15] Table 1 presents the general characteristics of both the laboratory-generated amorphous SOA and organic-dominated particles collected during the CalNex campaign (Wang et al., submitted manuscript, 2012). The O/C ratio was derived from c-ToF-AMS spectra using the technique described by *Aiken et al.* [2008], who developed an empirical correlation between O/C ratio and the fraction of AMS signal at $m/z = 44$ ($f44$): O/C = 3.82 × $f44$ + 0.0794. At OH exposures of 2.8×10^{11}, 1.0×10^{12}, and 2.2×10^{12} molec cm^{-3} s, corresponding SOA O/C ratios were 0.27, 0.54, and 1.0. The upper limit for the 1σ uncertainty in O/C ratio (absolute accuracy) is estimated to be $\pm 30\%$, where the precision error is much smaller (10%) [*Massoli et al.*, 2010].

The effective density (ρ_{org}) of SOA particles was calculated from the ratio of modal AMS vacuum aerodynamic diameter and modal SMPS mobility diameter measured during particle collection, assuming spherical particles [*DeCarlo et al.*, 2004], yielding SOA ρ_{org} values of about 1.3 g cm^{-3}. The measured κ value ranges from 0.14 to 0.24 for the investigated SOA particles for O/C ratios of 0.27 to 1.0.

3.2. Water Uptake and Heterogeneous Ice Nucleation

[16] Figure 2 summarizes the mean onset conditions ($\pm 1\sigma$) of water uptake, immersion freezing, and deposition ice nucleation by laboratory-generated amorphous SOA particles with O/C ratio from 0.27 to 1.0. Laboratory-generated amorphous SOA particles with different O/C ratios acted as IN at $T > 230$ K via water uptake at RH ranging from 83 to 93%, followed by immersion freezing at RH_{ice} ranging from 135 to 148% between 230 and 241 K. As shown in Figure 2, SOA particles with high O/C ratio took up water at mean RH values of 80–85% between 230 and 250 K. For most of the cases, between 242 and 230 K, immersion freezing occurred at 135–141% RH_{ice} after water uptake. SOA particles with medium and low O/C ratios also took up water but at higher RH values compared to particles with high O/C ratio.

Between 230 and 242 K, SOA particles with medium and low O/C ratios also initiated ice nucleation via immersion freezing at higher RH_{ice} after water uptake. For all the SOA particle samples, no ice nucleation was observed above 242 K.

[17] For $T < 230$ K, SOA particles with different O/C ratios nucleated ice via deposition freezing at mean RH_{ice} values of 136 to 152% as shown in Figure 2, but minimum RH_{ice} values were as low as 123% (not shown). In general, the SOA particles with different O/C ratios nucleated ice at very similar mean RH_{ice} values and thus exhibited similar deposition ice nucleation efficiencies, independent of O/C ratio. For all investigated particles it appears that the mean onset RH_{ice} value increases from ~140% at 225 K to ~150% at 203 K. This range of RH_{ice} is ~10–15% lower than the homogeneous freezing limit, indicating the SOA particles' potential to influence ice cloud formation mechanisms at low temperatures.

[18] For comparison, Figure 2 also shows the ranges of onset conditions for water uptake, immersion freezing, and deposition ice nucleation by ambient particles collected in Los Angeles during the CalNex 2010 field study (Wang et al., submitted manuscript, 2012). The particles were collected by a cascade multi-orifice uniform deposition impactor at the ground site on May 19. Single particle analyses using computer controlled scanning electron microscopy with energy dispersive analysis of X-ray (CCSEM/EDX) and scanning transmission X-ray microscopy with near edge X-ray absorption fine structure spectroscopy (STXM/NEXAFS) showed that the samples were dominated by organic-coated particles. Majority of the particles can be characterized as soot coated with organic carbon, soot/inorganic material coated with organic carbon, or pure organics without inclusions (Wang et al., submitted manuscript, 2012). The bulk non-refractory particles exhibited an average O/C ratio of 0.41 ± 0.12 (P. L. Hayes et al., Aerosol composition in Los Angeles During the 2010 CalNex Campaign Studied by High Resolution Aerosol Mass Spectrometry, submitted to *Journal of Geophysical Research*, 2012). The organic coatings were most likely due to the enhanced photochemical processes and formation of SOA from anthropogenic emissions [*Veres et al.*, 2011; Wang et al., submitted manuscript, 2012].

[19] As shown in Figure 2, these field-collected particles acted as IN via water uptake at RH ranging from 84 to 87%, followed by immersion freezing at RH_{ice} ranging from 138 to 146% (93% to 100% RH at $T = 230$–242 K) (Wang et al., submitted manuscript, 2012). These ambient particles showed very similar onsets of water uptake compared to laboratory-generated SOA particles with low (0.27) and medium (0.54) O/C ratios. They also showed similar onsets of immersion freezing between 230 and 242 K compared to SOA particles. For higher temperatures between 243 and 250 K only, the ambient particles initiated immersion freezing at water saturation. This is most likely due to the presence of soot or inorganic inclusions acting as IN subsequent to deliquescence of the coating material on the ambient particles (Wang et al., submitted manuscript, 2012). The ambient particles nucleated ice via deposition mode at mean RH_{ice} ranging from 134 to 150% ($T = 207$–226 K). Previous ice nucleation studies performed on laboratory generated organic particles cannot explain water uptake and immersion

freezing (see Figure S1) as well as deposition ice nucleation (see auxiliary material Figure S2) observed for the Los Angeles ambient particles. However, as shown in Figure 2, the investigated amorphous SOA particles exhibited remarkably similar water uptake and IN onsets compared to the Los Angeles ambient particles.

[20] We examined factors that influence the ice nucleation efficiency of SOA particles. One of these is the relationship between the measured O/C ratio of the SOA and water uptake in the subsaturated regime, that is, immersion freezing and deposition ice nucleation. Figure 2 shows data from separate experiments using SOA with O/C ratios of 0.27, 0.54, and 1.0. At ~247 K, water uptake occurs at RH ~93% (O/C = 0.27), 87% (O/C = 0.54), and 80% (O/C = 1.0), confirming that SOA hygroscopicity increases with oxidation level [*Jimenez et al.*, 2009; *Massoli et al.*, 2010]. These data bound the ambient Los Angeles measurements described earlier, in which water uptake was observed at RH ranging from 84 to 87% ($T = 230$–242 K). Below 240 K, the correlation of water uptake with O/C ratio becomes weaker as temperature decreases. The most likely explanation for this behavior is that water uptake is more affected by the lower D_{H_2O} at lower temperatures which results in slower diffusion of water molecules into the first particle layers [*Koop et al.*, 2011; *Shiraiwa et al.*, 2011; *Zobrist et al.*, 2011] irrespective of particle bulk O/C ratio. Because immersion freezing is preceded by water uptake, the immersion freezing efficiency is also positively correlated with O/C ratio. However, the correlation of immersion freezing with O/C ratio is weaker at temperatures below 240 K, possibly for similar reasons as given above for water uptake.

[21] The characteristic time of mass-transport and mixing of water molecules by molecular diffusion (τ) in aerosol particles was calculated as $\tau = D^2/4\pi^2 D_{H_2O}$ [*Shiraiwa et al.*, 2011]. Estimation of D_{H_2O} for varying temperature follows the approach by *Zobrist et al.* [2011] which is based on amorphous sucrose particles. D_{H_2O} decreases from ~10^{-13} to ~10^{-14} cm^2 s^{-1} as the temperature decreases from 246 to 231 K, yielding characteristic water diffusive mixing times (τ) of a few hundreds of seconds to over an hour, respectively, for the SOA particles with size of ~0.7–1.1 μm. Hence, for T above 246 K (i.e., above the homogeneous freezing limit) D_{H_2O} was likely sufficiently large and τ sufficiently small to result in complete deliquescence of the particles before RH reached water saturation under our experimental conditions. At lower temperatures between 230 and 242 K, the amorphous solid particles were not completely deliquesced due to the gradual deliquescence process (moisture-induced phase transition) [*Mikhailov et al.*, 2009; *Koop et al.*, 2011] and exhibit a core/shell structure. Thus, immersion freezing was initiated by the residual cores. At even lower temperatures, where D_{H_2O} can be as low as ~10^{-15} cm^2 s^{-1} and τ over one day, the onset of deposition ice nucleation was not correlated with the SOA O/C ratio since, most likely, water uptake was significantly hindered by the extremely low D_{H_2O}.

3.3. Glass Transition Temperature of Amorphous Organic Particles

[22] To investigate the role of particle phase states in water uptake and ice nucleation, T_g was used as a representative temperature to determine the phase state of particles. A
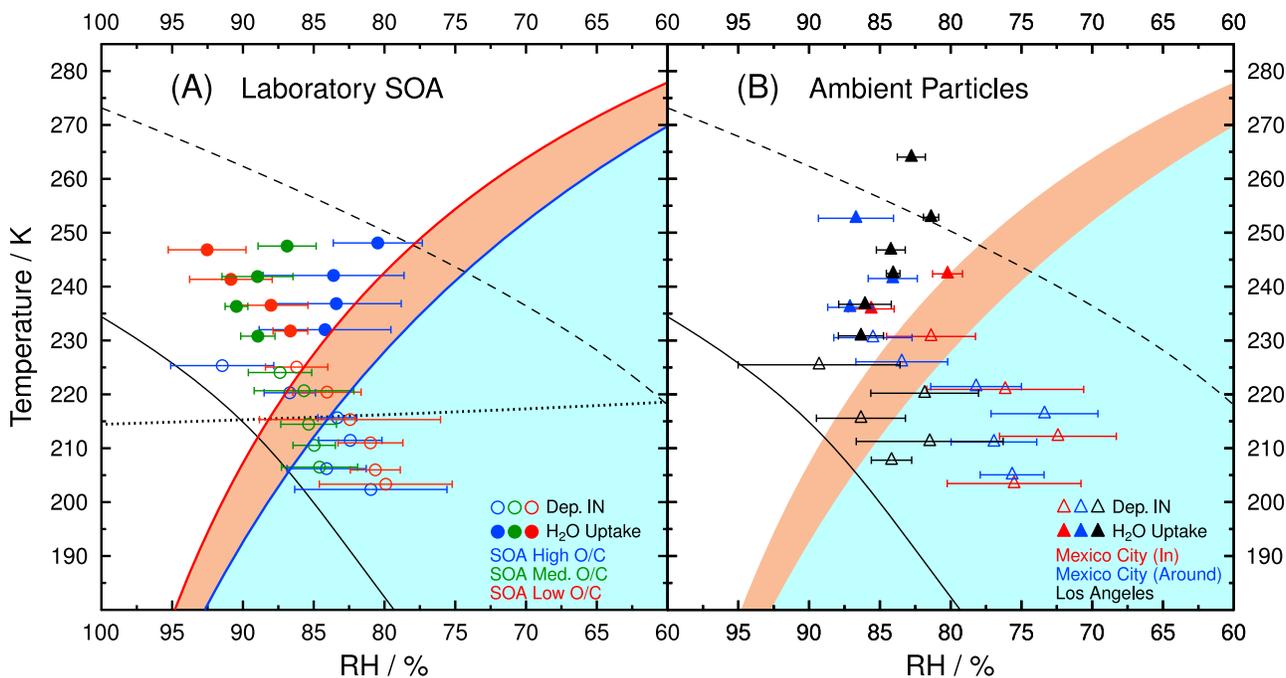
Figure 3. (a) The range of predicted glass transition temperatures (T_g) for the laboratory-generated amorphous solid SOA particles as a function of RH (brown area). The mean onset conditions for deposition ice nucleation (open circles) and water uptake (solid circles) by solid SOA particles from Figure 2 are shown. The blue and red lines represent the predicted $T_g(RH)$ for SOA particles with high and low O/C ratios, respectively. The dashed and solid black lines represent the ice melting and homogeneous freezing curve, respectively [Koop et al., 2000]. The dotted line indicates a typical experimental trajectory. The cyan area indicates conditions for which the studied SOA is in a solid state. (b) The onset conditions ($\pm 1\sigma$) for deposition ice nucleation and water uptake by ambient particles collected in (red) and around (blue) Mexico City [Knopf et al., 2010] and Los Angeles (black) (Wang et al., submitted manuscript, 2012) are given as open and solid triangles, respectively. All other lines are the same as in Figure 4a.

range of T_g for the investigated SOA particles as a function of RH, $T_g(RH)$, was estimated following the methods by *Koop et al.* [2011].

[23] T_g of aerosol particles is strongly affected by the particles' water content (RH) and temperature. Water serves as a plasticizer and reduces $T_g(RH)$ of particles below $T_g(RH = 0\%)$ [*Koop et al.*, 2011]. In this study, the upper limit of T_g as a function of RH for organic particles was determined using

$$T_g(RH) = \frac{w_w T_{g,w} + w_{org} T_g(RH = 0\%)/k_{GT}}{w_w + w_{org}/k_{GT}}, \qquad (3)$$

$$RH/100 = a_w = \left(1 + \kappa_{org}\frac{\rho_w}{\rho_{org}}\frac{w_{org}}{w_w}\right)^{-1}, \qquad (4)$$

where w_w and w_{org} are the mass fractions of water and organic matter, respectively, $T_{g,w}$ is the T_g of 136 K for pure water, k_{GT} is the Gordon-Taylor constant for the specific water/organic system representing the interaction between water and organic solute, a_w is the water activity of the particle (equivalent to RH at equilibrium conditions), κ_{org} is the CCN-derived hygroscopicity parameter of the organic fraction, and ρ_w and ρ_{org} are the density of water and organic material, respectively. a_w calculated from κ_{org} is strictly only

valid at the temperature at which κ_{org} has been obtained. Here we assume that a_w does not change significantly for constant solution composition with decreasing temperature [*Koop et al.*, 2000]. However, it has been shown that a_w can change when temperature decreases for inorganic and organic aqueous solutions of fixed composition [*Zobrist et al.*, 2003, 2008; *Knopf and Lopez*, 2009; *Knopf and Rigg*, 2011]. If and how a_w changes with temperature for applied laboratory-generated SOA particles is not known and should be investigated in future research.

[24] ρ, κ_{org}, k_{GT}, and the glass transition temperature of the pure dry organic particle, $T_g(RH = 0\%)$, are the necessary parameters to predict T_g as function of RH and temperature, i.e. $T_g(T, RH)$.

[25] According to equations (3) and (4), $T_g(RH)$ can be expressed as

$$T_g(RH) = \frac{T_{g,w}k_{GT} + f(RH)T_g(RH = 0\%)}{k_{GT} + f(RH)}, \qquad (5)$$

where

$$f(RH) = \frac{w_{org}}{w_w} = \frac{100 - RH}{RH}\frac{1}{\kappa_{org}}\frac{\rho_{org}}{\rho_w}. \qquad (6)$$

$T_g(RH)$ for SOA particles was predicted using the experimentally derived parameters summarized in Table 1. For

SOA particles, ρ_{org} and κ_{org} were measured or derived during particle collection. Due to the lack of k_{GT} data for secondary organic materials, *Koop et al.* [2011] suggest to use $k_{GT} = 2.5 \pm 1$ as best estimates for SOA related compounds based on experimental data determined by *Zobrist et al.* [2008] for various organic compounds. In this study, a k_{GT} of 1.5 was used as a lower bound for the SOA and Suwannee River Fulvic Acid (SRFA) particles. A lower k_{GT} value will result in higher T_g. Thus, the present estimate of $T_g(RH)$ should be considered as an upper limit. Currently, $T_g(RH = 0\%)$ values for SOA particles are not available [*Koop et al.*, 2011]. As discussed above, SOA particles generated at 298 K and 35% *RH* adopt an amorphous semi-solid state. Thus, T_g of 298 K at 35% *RH* was used as an upper constraint along with $T_{g,w}$ (i.e., 136 K at 100% *RH*) to derive $T_g(RH = 0\%)$ using equations (5) and (6). Then $T_g(RH = 0\%)$ were applied to predict the upper limit of $T_g(RH)$. The $T_g(RH = 0\%)$ for the investigated SOA particles with different O/C ratios are listed in Table 1.

[26] Figure 3 shows $T - RH$ phase diagrams for naphthalene SOA with O/C ratios of 0.27 (red line) and 1.0 (blue line). These curves bound the phase space in which the investigated SOA particles are expected to transition from a liquid/semi-solid (white region) to a solid (cyan region) [*Koop et al.*, 2011]. The brown region indicates the range of predicted $T_g(RH)$ for the SOA particles with different O/C ratios. Within this region, Figure 3 shows that for a specific T and *RH*, SOA particles with lower O/C ratio are more likely to be in a solid phase than SOA particles with higher O/C ratio.

[27] Figure 3 shows the onset conditions of water uptake (closed symbols) and deposition ice nucleation (open symbols) of the SOA particles (Figure 3a) and ambient particles [*Knopf et al.*, 2010; Wang et al., submitted manuscript, 2012] (Figure 3b) as a function of T and *RH*. As is evident for the great majority of the particles, water uptake occurred while the organic materials were liquid/semi-solid (T higher than $T_g(RH)$), whereas deposition ice nucleation was observed once the organic material are solid ($T < T_g$). For observed deposition ice nucleation events above $T_g(RH)$), e.g. at 225 K for SOA particles with high O/C ratio (5 out of 7 ice nucleation events), we speculate that this might be due to the competition between water uptake and ice nucleation when particles existed in a semi-solid (i.e. highly viscous) state at T only few degrees higher than $T_g(RH)$. In other words, the timescale to initiate deposition ice nucleation may be shorter than for dissolving the first organic layers of the particles. Figure 3a suggests that particle viscosity and phase influence ice formation by modifying T_g. To the extent that T_g values derived for the naphthalene SOA particles are applicable to ambient conditions, Figure 3b suggests that the ambient particles sampled in Mexico City [*Knopf et al.*, 2010] and Los Angeles (Wang et al., submitted manuscript, 2012) might also exist as semi-solids or solids at the onset conditions of deposition ice nucleation.

3.4.   Comparison With Previous Ice Nucleation Studies
### 3.4.1.   Comparison With Studies Using Laboratory-Generated SOA
[28] Few previous studies have investigated the ice nucleation efficiency of SOA particles over a more limited range of conditions [*Wagner et al.*, 2007; *Prenni et al.*, 2009b;

Möhler et al., 2008]. *Möhler et al.* [2008] found that the RH_{ice} threshold for α-pinene SOA was approximately 170% at 205 K, which was above the homogenous freezing limit. In this work, the mean RH_{ice} threshold for naphthalene SOA ranged from 145 to 152% (via deposition ice nucleation) for $T = 202$–206 K. If the α-pinene SOA particles produced by *Möhler et al.* [2008] were liquid at 205 K, this might explain their poor ice nucleation efficiency. *Koop et al.* [2011] measured and predicted T_g of several α-pinene oxidation products (pinonaldehyde, pinonic acid, pinic acid) over the range from 175 to 268 K, which support the possibility that the SOA particles studied by *Möhler et al.* [2008] were liquid or semi-solid. It should be noted that the α-pinene SOA particles applied by *Möhler et al.* [2008] are 4–6 times smaller in diameter than the particles employed in this study. According to classical nucleation theory, smaller particles of same type or less total particle surface area available can result in higher ice nucleation onsets [*Pruppacher and Klett*, 1997; *Kanji et al.*, 2008; *Kanji and Abbatt*, 2010]. *Prenni et al.* [2009b] showed that at 243 K, alkene SOA particles generated from ozonolysis of mono- and sesquiterpenes, cyclic alkenes, and linear alkenes did not induce freezing. In our experiments, naphthalene SOA initiated immersion freezing for T below 241 K; above 241 K, the particles only took up water but did not nucleate ice, consistent with results of *Prenni et al.* [2009b].

3.4.2.   Comparison With Studies Using Organic Particle Surrogates
[29] Laboratory-generated particles consisting of single or multiple organic compounds are often used as a surrogate of atmospheric organic particles, such as dicarboxylic acid and fulvic acid. Fulvic acid, such as SRFA, is often applied as surrogates of soluble atmospheric HUmic-LIke Substances (HULIS) which represent multifunctional organic material with high molecular weight typical of biomass burning aerosol [e.g., *Fuzzi et al.*, 2001; *Dinar et al.*, 2006a; *Graber and Rudich*, 2006; *Wang and Knopf*, 2011]. SRFA exhibited a bulk O/C ratio of 0.57 [*Dinar et al.*, 2006a] similar to the investigated SOA particles with medium O/C ratio (0.54). Previous studies have shown that SRFA particles can adopt an amorphous solid state at room temperature [*Koop et al.*, 2011; *Young and Leboeuf*, 2000]. *Wang and Knopf* [2011] showed that unoxidized and O_3-oxidized SRFA particles can serve as efficient IN via immersion freezing and deposition ice nucleation for different temperature regimes. To further investigate the connection between particle phase and the different nucleation modes, $T_g(RH)$ for SRFA particles was calculated using experimentally determined ρ_{org} of ~1.5 [*Dinar et al.*, 2006a], κ_{org} of 0.025–0.077 [*Dinar et al.*, 2006b, 2006a; *Svenningsson et al.*, 2006; *Petters et al.*, 2009], and $T_g(RH = 0\%)$ of 309 K [*Young and Leboeuf*, 2000] (Table 1). SOA particles showed very similar deposition ice nucleation onsets compared to unoxidized and O_3-oxidized SRFA particles below 230 K as shown in Figure 4. The majority of water uptake by SRFA particles was observed above the $T_g(RH)$. Most of the deposition ice nucleation events were observed below or within the range of predicted $T_g(RH)$. Again, the few observed deposition ice nucleation events above $T_g(RH)$ might be due to competition between water uptake and ice nucleation processes. Overall, the observed onset conditions of water uptake and deposition ice nucleation by SRFA particles also follow the
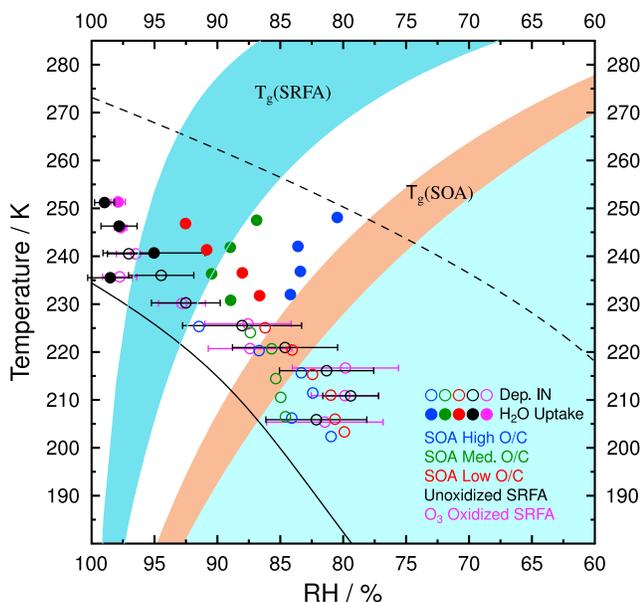
Figure 4. The range of predicted upper limits of T_g for SRFA particles as a function of RH. Mean onset conditions for deposition ice nucleation (open circles) and water uptake (solid circles) by unoxidized (black) and O_3-oxidized (magenta) SRFA particles are given as a function of RH [*Wang and Knopf*, 2011]. Error bars represent $\pm 1\sigma$. Dark cyan area is the predicted T_g for SRFA particles using κ_{org} of 0.025–0.077. The remaining lines and symbols are the same as in Figure 3.

predicted $T_g(RH)$ of SRFA particles. Interestingly, SRFA particles nucleated ice via deposition mode until higher temperatures and took up water at higher RH compared to SOA particles. This is most likely due to the higher $T_g(RH)$ of SRFA compared to the investigated SOA particles.

[30] *Murray et al.* [2010] showed that amorphous solid citric acid particles can nucleate ice via deposition mode below 212 K, but above 212 K, the citric acid particles adopted an aqueous state and nucleated ice homogeneously. Most recently, *Wilson et al.* [2012] and *Wagner et al.* [2012] found that pure organic compounds of raffinose, HMMA, and levoglucosan and a multi-component organic/inorganic mixture (Raffinose/M5AS) can nucleate ice heterogeneously below the respective $T_g(RH)$ [*Zobrist et al.*, 2008]. Auxiliary material Figures S2 and S3 compare the ice nucleation onsets of amorphous SOA and particles collected during the CalNex field campaign with ice nucleation onsets of laboratory-generated organic particles serving as proxies of atmospheric aerosol particles. The data obtained from previous studies are shown in auxiliary material Figures S2b and S3b which are adapted from *Knopf et al.* [2010]. The majority of the previous laboratory-generated organic or organic-containing particles are either very efficient IN which activate at $\sim$110% RH_{ice} or less efficient IN which activate close to water saturation or at the homogeneous freezing limit. Clearly, the observed ice nucleation onsets of laboratory-generated organic or organic-containing particle surrogates are in contrast to the observed onsets of naphthalene SOA particles and the ambient organic-dominated particles collected in Los Angeles.

3.4.3. Comparison to Ice Nucleation Efficiency of Mineral Dust and Ammonium Sulfate

[31] For the majority of the deposition ice nucleation experiments involving the laboratory-generated SOA particles and the organic particles collected in Los Angeles and in and around Mexico City, when repeated at same temperature using same sample, ice crystals did not form on the same particles [*Knopf et al.*, 2010; Wang et al., submitted manuscript, 2012]. Whereas for the mineral dust, such as Arizona test dust [*Knopf and Koop*, 2006] and Kaolinite [*Knopf et al.*, 2010; *Wang and Knopf*, 2011] deposition ice nucleation was, for the majority of the cases, initiated by the same particle when the ice nucleation experiments were repeated at the same temperature. These findings indirectly corroborate that particle morphology, which also governs deposition ice nucleation [*Pruppacher and Klett*, 1997], changes due to hydration and dehydration cycles as observed at room temperature [*Mikhailov et al.*, 2009] and when the organic particle transitions from solid to liquid and from liquid to solid (i.e. exposure to temperatures and/or humidity above and below the glass transition temperature, respectively) at the beginning of each experiment. This is in clear contrast to inorganic material such as mineral dust which seems not to experience significant morphological changes as temperature is varied.

[32] In this study, deposition ice nucleation of SOA particles was also analyzed with regard to classical nucleation theory and singular hypothesis providing estimates of heterogeneous ice nucleation rate coefficients and cumulative IN spectra, respectively. The analytical methods and results, including the IN activated fraction, are given in the auxiliary material. Classical nucleation theory provides a parameter, contact angle (θ), which determines IN efficiency of particles and can be used as a parameter to compare the ice nucleation efficiencies of different types of IN. A smaller θ corresponds to a more efficient ice nucleus. However, comparison of θ of different IN may only be meaningful when similar IN particle size and total particulate surface area are employed. Previous studies suggested that a diameter of about 100–200 nm represents the threshold size at which a particle could initiate ice nucleation [e.g., *Pruppacher and Klett*, 1997; *Marcolli et al.*, 2007]. RH_{ice} onset and corresponding contact angle can significantly depend on particle size for particles smaller than 200 nm whereas for particles above 200 nm this dependency may be less pronounced [*Welti et al.*, 2009; *Kanji and Abbatt*, 2010]. For a first order comparison of ice nucleation efficiencies, auxiliary material Table S1 lists the θ for the investigated SOA particles, ammonium sulfate particles, and several types of mineral dust from previous studies which applied similar total particulate surface areas and particle sizes above 200 nm. The SOA particles exhibit a mean θ of $\sim$(25.4–27.9) $\pm$ 1.3° for deposition ice nucleation. Quartz, calcite, and kaolinite listed in Table S1 are often found in atmospheric dust sources [*Claquin et al.*, 1999] and airborne dust [e.g., *Glaccum and Prospero*, 1980]. The SOA particles exhibit similar θ compared to some types of mineral dust, such as quartz (26.3–27.1°) and calcite (θ = 24.9–26.4°) [*Eastwood et al.*, 2008]. Kaolinite (θ = 6–18.5°) and muscovite (θ = 6.2–10.7°) are more efficient IN [e.g., *Eastwood et al.*, 2008; Wang et al., submitted manuscript, 2012; *Welti et al.*, 2009]. *Shilling et al.* [2006] determined a mean θ of $\sim$14 $\pm$ 2.5° for ammonium sulfate particles indicating a

higher ice nucleation efficiency compared to SOA particles. However, if the mineral dust with high ice nucleation efficiency or crystalline sulfate particles are coated with secondary organic material, the particle ice nucleation efficiency will be determined by the SOA coating as evident from field-collected particles [*Knopf et al.*, 2010].

4. Summary and Conclusions

[33] Amorphous SOA particles generated from the oxidation of naphthalene with OH radicals demonstrate the potential to act as deposition IN at temperatures below 230 K and below the homogeneous freezing limit. Water uptake was observed above 230 K followed by immersion freezing at temperatures between 230 and 245 K. The bulk atomic oxygen-to-carbon (O/C) ratio of these SOA particles did not show a significant effect on deposition ice nucleation within the experimental uncertainty but affected initial water uptake. Above 230 K particles with higher O/C ratio took up water at lower *RH* than particles with low O/C ratio. The upper limits of glass transition temperature (T_g) for the laboratory-generated amorphous SOA particles were derived as a function of *RH* based on the method proposed by *Koop et al.* [2011]. $T_g(RH)$ for SOA particles correlates with the observed different heterogeneous ice nucleation pathways and water uptake that particles initiated deposition ice nucleation and took up water below and above $T_g(RH)$, respectively.

[34] Urban ambient particles impacted or formed from anthropogenic precursors in two megacities exhibited similar water uptake and ice nucleation properties as the investigated SOA particles. The efficiency of investigated SOA particles to act as IN under atmospherically relevant conditions modulated by their glass transition points (T_g and *RH*) provides an possible explanation of the ice nucleation efficiency of ambient particles. Previous studies have shown that pollutants from Los Angeles Basin can be transported into free troposphere [e.g., *Langford et al.*, 2010; *Neuman et al.*, 2012]. *Neuman et al.* [2012] showed that pollutants from aged regional emissions were transported into free troposphere on May 19 over the Los Angeles Basin which could be due to the slow injection from boundary layer. Also *Heald et al.* [2011] indicate the presence of a significant fraction of SOA above the boundary layer. SOA particles and urban ambient particles that exist as semi-solids or solids may therefore play a role in the formation of cirrus and mixed-phase clouds in the atmosphere, implying a potential link of human and biogenic activities with cloud formation processes and climate. The results presented in this study suggest that amorphous SOA may need to be considered as IN in the next generation of cloud and climate models in addition to typical IN such as mineral dust particles. Further climate and cloud modeling studies are needed to determine the potential effects of SOA acting as IN on the hydrological cycle and radiative forcing. The findings may also be applicable to SOA formed from other anthropogenic and biogenic precursors with a similar range of T_g, and this topic will be examined in future work.

References

Abbatt, J. P. D., S. Benz, D. J. Cziczo, Z. Kanji, U. Lohmann, and O. Möhler (2006), Solid ammonium sulfate aerosols as ice nuclei: A pathway for cirrus cloud formation, *Science*, *313*, 1770–1773.

Aiken, A. C., et al. (2008), O/C and OM/OC ratios of primary, secondary, and ambient organic aerosols with high-resolution time-of-flight aerosol mass spectrometry, *Environ. Sci. Technol.*, *42*(12), 4478–4485, doi:10.1021/es703009q.

Baker, M. B., and T. Peter (2008), Small-scale cloud processes and climate, *Nature*, *451*, 299–300, doi:10.1038/nature06594.

Baustian, K. J., D. J. Cziczo, M. E. Wise, K. A. Pratt, G. Kulkarni, A. G. Hallar, and M. A. Tolbert (2012), Importance of aerosol composition, mixing state, and morphology for heterogeneous ice nucleation: A combined field and laboratory approach, *J. Geophys. Res.*, *117*, D06217, doi:10.1029/2011JD016784.

Chen, T., W. B. Rossow, and Y. Zhang (2000), Radiative effects of cloud-type variations, *J. Clim.*, *13*(1), 264–286, doi:10.1175/1520-0442(2000)013<0264:REOCTV>2.0.CO;2.

Chen, Y., S. M. Kreidenweis, L. M. McInnes, D. C. Rogers, and P. J. DeMott (1998), Single particle analyses of ice nucleating aerosols in the upper troposphere and lower stratosphere, *Geophys. Res. Lett.*, *25*(9), 1391–1394, doi:10.1029/97GL03261.

Claquin, T., M. Schulz, and Y. Balkanski (1999), Modeling the mineralogy of atmospheric dust sources, *J. Geophys. Res.*, *104*(D18), 22,243–22,256, doi:10.1029/1999JD900416.

Cziczo, D. J., K. D. Froyd, S. J. Gallavardin, O. Moehler, S. Benz, H. Saathoff, and D. M. Murphy (2009), Deactivation of ice nuclei due to atmospherically relevant surface coatings, *Environ. Res. Lett.*, *4*(4), 044013, doi:10.1088/1748-9326/4/4/044013.

Debenedetti, P., and F. Stillinger (2001), Supercooled liquids and the glass transition, *Nature*, *410*(6825), 259–267, doi:10.1038/35065704.

de Boer, G., H. Morrison, M. D. Shupe, and R. Hildner (2011), Evidence of liquid dependent ice nucleation in high-latitude stratiform clouds from surface remote sensors, *Geophys. Res. Lett.*, *38*, L01803, doi:10.1029/2010GL046016.

DeCarlo, P. F., J. G. Slowik, D. R. Worsnop, P. Davidovits, and J. L. Jimenez (2004), Particle morphology and density characterization by combined mobility and aerodynamic diameter measurements. Part 1: Theory, *Aerosol Sci. Technol.*, *38*(12), 1185–1205.

DeMott, P. J., D. J. Cziczo, A. J. Prenni, D. M. Murphy, S. M. Kreidenweis, D. S. Thomson, R. Borys, and D. C. Rogers (2003), Measurements of the concentration and composition of nuclei for cirrus formation, *Proc. Natl. Acad. Sci. U. S. A.*, *100*(25), 14,655–14,660, doi:10.1073/pnas.2532677100.

Dinar, E., T. F. Mentel, and Y. Rudich (2006a), The density of humic acids and humic like substances (HULIS) from fresh and aged wood burning and pollution aerosol particles, *Atmos. Chem. Phys.*, *6*(12), 5213–5224, doi:10.5194/acp-6-5213-2006.

Dinar, E., I. Taraniuk, E. R. Graber, S. Katsman, T. Moise, T. Anttila, T. F. Mentel, and Y. Rudich (2006b), Cloud condensation nuclei properties of model and atmospheric HULIS, *Atmos. Chem. Phys.*, *6*(9), 2465–2482, doi:10.5194/acp-6-2465-2006.

Drewnick, F., et al. (2005), A new time-of-flight aerosol mass spectrometer (TOF-AMS) - Instrument description and first field deployment, *Aerosol Sci. Technol.*, *39*(7), 637–658, doi:10.1080/02786820500182040.

Eastwood, M. L., S. Cremel, C. Gehrke, E. Girard, and A. K. Bertram (2008), Ice nucleation on mineral dust particles: Onset conditions, nucleation rates and contact angles, *J. Geophys. Res.*, *113*, D22203, doi:10.1029/2008JD010639.

Froyd, K. D., D. M. Murphy, T. J. Sanford, D. S. Thomson, J. C. Wilson, L. Pfister, and L. Lait (2009), Aerosol composition of the tropical upper troposphere, *Atmos. Chem. Phys.*, *9*(13), 4363–4385, doi:10.5194/acp-9-4363-2009.

Froyd, K. D., D. M. Murphy, P. Lawson, D. Baumgardner, and R. L. Herman (2010), Aerosols that form subvisible cirrus at the tropical tropopause, *Atmos. Chem. Phys.*, *10*(1), 209–218, doi:10.5194/acp-10-209-2010.

Fuzzi, S., S. Decesari, M. C. Facchini, E. Matta, M. Mircea, and E. Tagliavini (2001), A simplified model of the water soluble organic component of atmospheric aerosols, *Geophys. Res. Lett.*, *28*(21), 4079–4082.

Glaccum, R., and J. Prospero (1980), Saharan aerosols over the tropical North Atlantic - Mineralogy, *Mar. Geol.*, 37(3–4), 295–321, doi:10.1016/0025-3227(80)90107-3.

Graber, E. R., and Y. Rudich (2006), Atmospheric HULIS: How humic-like are they? A comprehensive and critical review, *Atmos. Chem. Phys.*, 6(3), 729–753, doi:10.5194/acp-6-729-2006.

Hallquist, M., et al. (2009), The formation, properties and impact of secondary organic aerosol: Current and emerging issues, *Atmos. Chem. Phys.*, 9(14), 5155–5236, doi:10.5194/acp-9-5155-2009.

Heald, C. L., et al. (2011), Exploring the vertical profile of atmospheric organic aerosol: Comparing 17 aircraft field campaigns with a global model, *Atmos. Chem. Phys.*, 11(24), 12,673–12,696, doi:10.5194/acp-11-12673-2011.

Jimenez, J. L., et al. (2009), Evolution of organic aerosols in the atmosphere, *Science*, 326(5959), 1525–1529, doi:10.1126/science.1180353.

Kanakidou, M., et al. (2005), Organic aerosol and global climate modelling: A review, *Atmos. Chem. Phys.*, 5(4), 1053–1123, doi:10.5194/acp-5-1053-2005.

Kang, E., M. J. Root, D. W. Toohey, and W. H. Brune (2007), Introducing the concept of potential aerosol mass (PAM), *Atmos. Chem. Phys.*, 7(22), 5727–5744, doi:10.5194/acp-7-5727-2007.

Kanji, Z. A., and J. P. D. Abbatt (2010), Ice nucleation onto Arizona Test Dust at cirrus temperatures: Effect of temperature and aerosol size on onset relative humidity, *J. Phys. Chem. A*, 114(2), 935–941, doi:10.1021/jp908661m.

Kanji, Z. A., O. Florea, and J. P. D. Abbatt (2008), Ice formation via deposition nucleation on mineral dust and organics: dependence of onset relative humidity on total particulate surface area, *Environ. Res. Lett.*, 3(2), 025004, doi:10.1088/1748-9326/3/2/025004.

Kärcher, B., and U. Lohmann (2003), A parameterization of cirrus cloud formation: Heterogeneous freezing, *J. Geophys. Res.*, 108(D14), 4402, doi:10.1029/2002JD003220.

Kärcher, B., and J. Ström (2003), The roles of dynamical variability and aerosols in cirrus cloud formation, *Atmos. Chem. Phys.*, 3(3), 823–838, doi:10.5194/acp-3-823-2003.

Kärcher, B., J. Hendricks, and U. Lohmann (2006), Physically based parameterization of cirrus cloud formation for use in global atmospheric models, *J. Geophys. Res.*, 111, D01205, doi:10.1029/2005JD006219.

Knopf, D. A., and T. Koop (2006), Heterogeneous nucleation of ice on surrogates of mineral dust, *J. Geophys. Res.*, 111, D12201, doi:10.1029/2005JD006894.

Knopf, D. A., and M. D. Lopez (2009), Homogeneous ice freezing temperatures and ice nucleation rates of aqueous ammonium sulfate and aqueous levoglucosan particles for relevant atmospheric conditions, *Phys. Chem. Chem. Phys.*, 11, 8056–8068, doi:10.1039/b903750k.

Knopf, D. A., and Y. J. Rigg (2011), Homogeneous ice nucleation from aqueous inorganic/organic particles representative of biomass burning: Water activity, freezing temperatures, nucleation rates, *J. Phys. Chem. A*, 115(5), 762–773, doi:10.1021/jp109171g.

Knopf, D. A., B. Wang, A. Laskin, R. C. Moffet, and M. K. Gilles (2010), Heterogeneous nucleation of ice on anthropogenic organic particles collected in Mexico City, *Geophys. Res. Lett.*, 37, L11803, doi:10.1029/2010GL043362.

Knopf, D. A., P. A. Alpert, B. Wang, and J. Y. Aller (2011), Stimulation of ice nucleation by marine diatoms, *Nat. Geosci.*, 4, 88–90, doi:10.1038/NGEO1037.

Koop, T., B. P. Luo, A. Tsias, and T. Peter (2000), Water activity as the determinant for homogeneous ice nucleation in aqueous solutions, *Nature*, 406, 611–614, doi:10.1038/35020537.

Koop, T., J. Bookhold, M. Shiraiwa, and U. Pöschl (2011), Glass transition and phase state of organic compounds: Dependency on molecular properties and implications for secondary organic aerosols in the atmosphere, *Phys. Chem. Chem. Phys.*, 13, 19,238–19,255, doi:10.1039/C1CP22617G.

Lambe, A. T., T. B. Onasch, P. Massoli, D. R. Croasdale, J. P. Wright, A. T. Ahern, L. R. Williams, D. R. Worsnop, W. H. Brune, and P. Davidovits (2011a), Laboratory studies of the chemical composition and cloud condensation nuclei (CCN) activity of secondary organic aerosol (SOA) and oxidized primary organic aerosol (OPOA), *Atmos. Chem. Phys.*, 11(17), 8913–8928, doi:10.5194/acp-11-8913-2011.

Lambe, A. T., et al. (2011b), Characterization of aerosol photooxidation flow reactors: heterogeneous oxidation, secondary organic aerosol formation and cloud condensation nuclei activity measurements, *Atmos. Meas. Tech.*, 4(3), 445–461, doi:10.5194/amt-4-445-2011.

Lance, S., J. Medina, J. Smith, and A. Nenes (2006), Mapping the operation of the DMT Continuous Flow CCN counter, *Aerosol Sci. Technol.*, 40(4), 242–254, doi:10.1080/02786820500543290.

Langford, A. O., C. J. Senff, R. J. Alvarez II, R. M. Banta, and R. M. Hardesty (2010), Long-range transport of ozone from the Los Angeles Basin: A case study, *Geophys. Res. Lett.*, 37, L06807, doi:10.1029/2010GL042507.

Mao, J., et al. (2009), Airborne measurement of OH reactivity during INTEX-B, *Atmos. Chem. Phys.*, 9(1), 163–173, doi:10.5194/acp-9-163-2009.

Marcolli, C., B. P. Luo, and T. Peter (2004), Mixing of the organic aerosol fractions: Liquids as the thermodynamically stable phases, *J. Phys. Chem. A*, 108(12), 2216–2224.

Marcolli, C., S. Gedamke, T. Peter, and B. Zobrist (2007), Efficiency of immersion mode ice nucleation on surrogates of mineral dust, *Atmos. Chem. Phys.*, 7(19), 5081–5091.

Martin, S. T. (2000), Phase transitions of aqueous atmospheric particles, *Chem. Rev.*, 100, 3403–3453.

Massoli, P., et al. (2010), Relationship between aerosol oxidation level and hygroscopic properties of laboratory generated secondary organic aerosol (SOA) particles, *Geophys. Res. Lett.*, 37, L24801, doi:10.1029/2010GL045258.

Mikhailov, E., S. Vlasenko, S. T. Martin, T. Koop, and U. Pöschl (2009), Amorphous and crystalline aerosol particles interacting with water vapor: Conceptual framework and experimental evidence for restructuring, phase transitions and kinetic limitations, *Atmos. Chem. Phys.*, 9(24), 9491–9522.

Möhler, O., S. Benz, H. Saathoff, M. Schnaiter, R. Wagner, J. Schneider, S. Walter, V. Ebert, and S. Wagner (2008), The effect of organic coating on the heterogeneous ice nucleation efficiency of mineral dust aerosols, *Environ. Res. Lett.*, 3(2), 1425–1435.

Murphy, D. M., and T. Koop (2005), Review of the vapour pressures of ice and supercooled water for atmospheric applications, *Q. J. R. Meteorol. Soc.*, 131(608), 1539–1565, doi:10.1256/qj.04.94.

Murray, B. J. (2008), Inhibition of ice crystallisation in highly viscous aqueous organic acid droplets, *Atmos. Chem. Phys.*, 8(17), 5423–5433, doi:10.5194/acp-8-5423-2008.

Murray, B. J., et al. (2010), Heterogeneous nucleation of ice particles on glassy aerosols under cirrus conditions, *Nat. Geosci.*, 3, 233–237.

Neuman, J. A., et al. (2012), Observations of ozone transport from the free troposphere to the Los Angeles basin, *J. Geophys. Res.*, 117, D00V09, doi:10.1029/2011JD016919.

Petters, M. D., and S. M. Kreidenweis (2007), A single parameter representation of hygroscopic growth and cloud condensation nucleus activity, *Atmos. Chem. Phys.*, 7(8), 1961–1971, doi:10.5194/acp-7-1961-2007.

Petters, M. D., S. M. Kreidenweis, A. J. Prenni, R. C. Sullivan, C. M. Carrico, K. A. Koehler, and P. J. Ziemann (2009), Role of molecular size in cloud droplet activation, *Geophys. Res. Lett.*, 36, L22801, doi:10.1029/2009GL040131.

Prenni, A. J., M. D. Petters, S. M. Kreidenweis, C. L. Heald, S. T. Martin, P. Artaxo, R. M. Garland, A. G. Wollny, and U. Pöschl (2009a), Relative roles of biogenic emissions and Saharan dust as ice nuclei in the Amazon basin, *Nat. Geosci.*, 2(6), 402–405, doi:10.1038/ngeo517.

Prenni, A. J., M. D. Petters, A. Faulhaber, C. M. Carrico, P. J. Ziemann, S. M. Kreidenweis, and P. J. DeMott (2009b), Heterogeneous ice nucleation measurements of secondary organic aerosol generated from ozonolysis of alkenes, *Geophys. Res. Lett.*, 36, L06808, doi:10.1029/2008GL036957.

Pruppacher, R. H., and J. D. Klett (1997), *Microphysics of Clouds and Precipitation*, Kluwer Acad., Dordrecht, Netherlands.

Renbaum, L. H., and G. D. Smith (2011), Artifacts in measuring aerosol uptake kinetics: The roles of time, concentration and adsorption, *Atmos. Chem. Phys.*, 11(14), 6881–6893, doi:10.5194/acp-11-6881-2011.

Roberts, G. C., and A. Nenes (2005), A continuous-flow streamwise thermal-gradient CCN chamber for atmospheric measurements, *Aerosol Sci. Technol.*, 39(3), 206–221.

Saukko, E., H. Kuuluvainen, and A. Virtanen (2012a), A method to resolve the phase state of aerosol particles, *Atmos. Meas. Tech.*, 5(1), 259–265, doi:10.5194/amt-5-259-2012.

Saukko, E., et al. (2012b), Humidity-dependent phase state of SOA particles from biogenic and anthropogenic precursors, *Atmos. Chem. Phys. Discuss.*, 12(2), 4447–4476, doi:10.5194/acpd-12-4447-2012.

Shilling, J. E., T. J. Fortin, and M. A. Tolbert (2006), Depositional ice nucleation on crystalline organic and inorganic solids, *J. Geophys. Res.*, 111, D12204, doi:10.1029/2005JD006664.

Shiraiwa, M., M. Ammann, T. Koop, and U. Pöschl (2011), Gas uptake and chemical aging of semisolid organic aerosol particles, *Proc. Natl. Acad. Sci. U. S. A.*, 108(27), 11,003–11,008, doi:10.1073/pnas.1103045108.

Shupe, M., S. Matrosov, and T. Uttal (2006), Arctic mixed-phase cloud properties derived from surface-based sensors at SHEBA, *J. Atmos. Sci.*, 63(2), 697–711, doi:10.1175/JAS3659.1.

Storelvmo, T., C. Hoose, and P. Eriksson (2011), Global modeling of mixed-phase clouds: The albedo and lifetime effects of aerosols, *J. Geophys. Res.*, 116, D05207, doi:10.1029/2010JD014724.

Svenningsson, B., et al. (2006), Hygroscopic growth and critical supersaturations for mixed aerosol particles of inorganic and organic compounds of atmospheric relevance, *Atmos. Chem. Phys.*, *6*(9), 1937–1952, doi:10.5194/acp-6-1937-2006.

Veres, P. R., et al. (2011), Evidence of rapid production of organic acids in an urban air mass, *Geophys. Res. Lett.*, *38*, L17807, 10.1029/2011GL048420.

Virtanen, A., et al. (2010), An amorphous solid state of biogenic secondary organic aerosol particles, *Nature*, *467*(7317), 824–827, doi:10.1038/nature09455.

Virtanen, A., et al. (2011), Bounce behavior of freshly nucleated biogenic secondary organic aerosol particles, *Atmos. Chem. Phys.*, *11*(16), 8759–8766, doi:10.5194/acp-11-8759-2011.

Wagner, R., S. Benz, O. Möhler, H. Saathoff, M. Schnaiter, and T. Leisner (2007), Influence of particle aspect ratio on the midinfrared extinction spectra of wavelength-sized ice crystals, *J. Phys. Chem. A*, *111*(50), 13,003–13,022, doi:10.1021/jp0741713.

Wagner, R., O. Möhler, H. Saathoff, M. Schnaiter, J. Skrotzki, T. Leisner, T. W. Wilson, T. L. Malkin, and B. J. Murray (2012), Ice cloud processing of ultra-viscous/glassy aerosol particles leads to enhanced ice nucleation ability, *Atmos. Chem. Phys. Discuss.*, *12*(4), 8921–8977, doi:10.5194/acpd-12-8921-2012.

Wang, B., and D. A. Knopf (2011), Heterogeneous ice nucleation on particles composed of humic-like substances impacted by O$_3$, *J. Geophys. Res.*, *116*, D03205, doi:10.1029/2010JD014964.

Welti, A., F. Lüönd, and U. Lohmann (2009), Influence of particle size on the ice nucleating ability of mineral dusts, *Atmos. Chem. Phys.*, *9*(18), 6705–6715, doi:10.5194/acp-9-6705-2009.

Wilson, T. W., et al. (2012), Glassy aerosols with a range of compositions nucleate ice heterogeneously at cirrus temperatures, *Atmos. Chem. Phys. Discuss.*, *12*(4), 8979–9033, doi:10.5194/acpd-12-8979-2012.

Wise, M. E., K. J. Baustian, and M. A. Tolbert (2010), Internally mixed sulfate and organic particles as potential ice nuclei in the tropical tropopause region, *Proc. Natl. Acad. Sci. U. S. A.*, *107*(15), 6693–6698, doi:10.1073/pnas.0913018107.

Young, K., and E. Leboeuf (2000), Glass transition behavior in a peat humic acid and an aquatic fulvic acid, *Environ. Sci. Technol.*, *34*(21), 4549–4553, doi:10.1021/es000889j.

Zobrist, B., U. Weers, and T. Koop (2003), Ice nucleation in aqueous solutions of poly[ethylene glycol] with different molar mass, *J. Chem. Phys.*, *118*(22), 10,254–10,261.

Zobrist, B., et al. (2006), Oxalic acid as a heterogeneous ice nucleus in the upper troposphere and its indirect aerosol effect, *Atmos. Chem. Phys.*, *6*, 3115–3129.

Zobrist, B., C. Marcolli, D. A. Pedernera, and T. Koop (2008), Do atmospheric aerosols form glasses?, *Atmos. Chem. Phys.*, *8*(17), 5221–5244.

Zobrist, B., V. Soonsin, B. P. Luo, U. K. Krieger, C. Marcolli, T. Peter, and T. Koop (2011), Ultra-slow water diffusion in aqueous sucrose glasses, *Phys. Chem. Chem. Phys.*, *13*, 3514–3526, doi:10.1039/C0CP01273D.